



Intraseasonal variability in the southwestern Arabian Sea and its relation to the seasonal circulation

Peter Brandt^{a,*}, Marcus Dengler^a, Angelo Rubino^b, Detlef Quadfasel^c,
Friedrich Schott^a

^a*Institut für Meereskunde an der Universität Kiel, Düsternbrooker Weg 20, 24105 Kiel, Germany*

^b*Institut für Meereskunde, Universität Hamburg, Troplowitzstr. 7, 22529 Hamburg, Germany*

^c*Niels Bohr Institutet for Astronomi, Fysik og Geofysik, Københavns Universitet, Juliane Maries Vej 30, 2100 Copenhagen, Denmark*

Abstract

An analysis of TOPEX/POSEIDON altimeter data and in situ current and temperature data obtained between April 1995 and October 1996 from a moored array shows strong intraseasonal fluctuations in the southwestern Arabian Sea, an oceanic region where the Great Whirl (GW), a predominantly wind-generated, very energetic anticyclone, is present during the Southwest Monsoon. Fluctuation periods between 30 and 50 days, up to 100 days during some years, are observed in the 8-year altimetric dataset, mostly during late summer and fall. These fluctuations are largest in a 1000 km-wide region off the Somali, Omani and Yemeni coasts north of 5°N, suggesting a local generation mechanism. The in situ data at different moorings show strong and coherent fluctuations that are characterized by southwestward phase propagation and northward energy propagation. Their periods range from 30 to 60 days and increase steadily from July 1995 to January 1996. In the first stage, these periods are at and below the cut-off period of freely propagating, first baroclinic mode Rossby waves, but approach this theoretical limit later in the year. Instabilities of the flow in the transition region between the Southern Gyre and the GW are likely sources of these fluctuations.

© 2003 Elsevier Science Ltd. All rights reserved.

1. Introduction

The Southern Gyre and the Great Whirl (GW) develop as large anticyclonic eddies in the southwestern Arabian Sea every year in response to the onset of the Southwest Monsoon (Swallow and Fieux, 1982). They are part of the Somali Current system, one of the most energetic regions of the World Ocean, where surface currents of more than 3 m/s have been observed (Swallow and Bruce, 1966; Schott, 1983; Fischer et al., 1996). Both eddies, in particular the GW, contribute substan-

tially to the upwelling along the northern Somali coast and to the eastward transport of cold water into the interior Arabian Sea. As such, the GW is part of the upward branch of the shallow tropical–subtropical circulation cell in the Indian Ocean and strongly affects the heat balance of the Arabian Sea (Schott et al., 2002).

The GW itself is limited to the upper 1000 m of the water column and current speeds above 1 m/s are only observed in the top 200 m (R. Schoenefeldt, pers. comm.). Most of the details concerning the generation, the persistence, and the decay or collapse of this eddy are still poorly understood (Schott and McCreary, 2001). Rapid changes such as a sudden northward propagation

*Corresponding author. Fax: +49-0431-597-3823.

E-mail address: pbrandt@ifm.uni-kiel.de (P. Brandt).

of the Southern Gyre and coalescence with the GW have been observed during several years (Evans and Brown, 1981), but in other years this two-gyre system remained in place and slowly decayed at the end of the Southwest Monsoon season. Until now this short-term and interannual variability could not be related in any simple way to variability in observed forcing fields, nor were numerical models able to realistically simulate the observed complex flow field in the area (Wirth et al., 2002). It appears, however, that intraseasonal variability plays a major role in the development of the seasonal cycle of the Somali Current.

Lighthill (1969) was the first to study the impact of equatorial Rossby waves on the development of the Somali Current. These waves are generated by winds associated with the Southwest Monsoon and lead to the development of a boundary current with a delay of about 1 month, due to the propagation time of the waves. The effect of remotely forced mid-latitude Rossby waves on the Somali Current was explored by Anderson and Rowlands (1976) who found them to accelerate the boundary current in the later phase of the Southwest Monsoon, whereas local wind forcing dominated right after the monsoon onset. The first time-series of currents, based on moored observations, showed fluctuations with typical periods of 50 days in the off-equatorial Somali Current that are believed to play an important role in the development of the GW (Schott and Quadfasel, 1982). However, with only about 3 months of observations, the time-series was too short to obtain significant statistics on these waves. In a more recent study, intraseasonal fluctuations emerged in a numerical ocean model of the Indian Ocean, which was forced with seasonal winds excluding periods shorter than 90 days (Sengupta et al., 2001). These fluctuations were interpreted as the result of hydrodynamical instabilities in the region of the GW.

Intraseasonal variability with planetary wave characteristics have thus been observed and modeled over the whole life cycle of the GW. It is, however, not clear how these fluctuations are generated or how they interact with the GW: Are they forced by the winds, either locally or remotely? Are they instabilities of the mean flow?

Do they contribute to the build-up of the GW, or do they lead to its decay and/or collapse?

In this investigation, we present an analysis of TOPEX/POSEIDON altimeter data and current and temperature data showing intraseasonal fluctuations in the GW region. The latter were collected during the World Ocean Circulation Experiment in 1995 and 1996 at the mooring array ICM-7 (positions shown in Fig. 1). The satellite data span a period of 8 years from 1992 to 2000.

2. Altimetric observations

The altimeter data, which were corrected for geophysical, tidal, sea state and instrumental effects as well as for orbit errors, are part of the TOPEX/POSEIDON sea-level anomaly products provided by Centre National d'Etudes Spatiales (CNES) and the National Aeronautics and Space Administration (NASA; AVISO, 1998). Here, we used the sea-surface height anomaly (SSHA) from along-track data (Fu et al., 1994) for the period October 1992–October 2000. Time-series of the along-track data were analyzed using a wavelet transform (see e.g. Torrence and Compo, 1998; Emery and Thomson, 2001). The adopted wavelet is a 'Morlet' wavelet, i.e. a cos-function that is modulated by a Gaussian distribution. The energy normalization was performed by dividing the time-series (i.e. the time-series at each along-track grid point) by the total variance of all time-series in the investigated region. The 95% significance level was calculated according to Torrence and Compo (1998).

A longitude–time plot of the SSHA at 7°N, which was derived from a 1° × 1° mapped field, is depicted in Fig. 2. The dominant signal is an annual cycle of westward propagating SSHAs. Brandt et al. (2002) interpreted these as annual Rossby waves of the first and second baroclinic mode that are radiated from the Indian subcontinent and that are continuously forced by the wind curl over the central Arabian Sea. In addition, near the coast of Somalia, smaller-scale signals of monthly to 2-monthly period were superimposed on the annual signal. When the SSHA data were high-pass filtered, their westward propagation

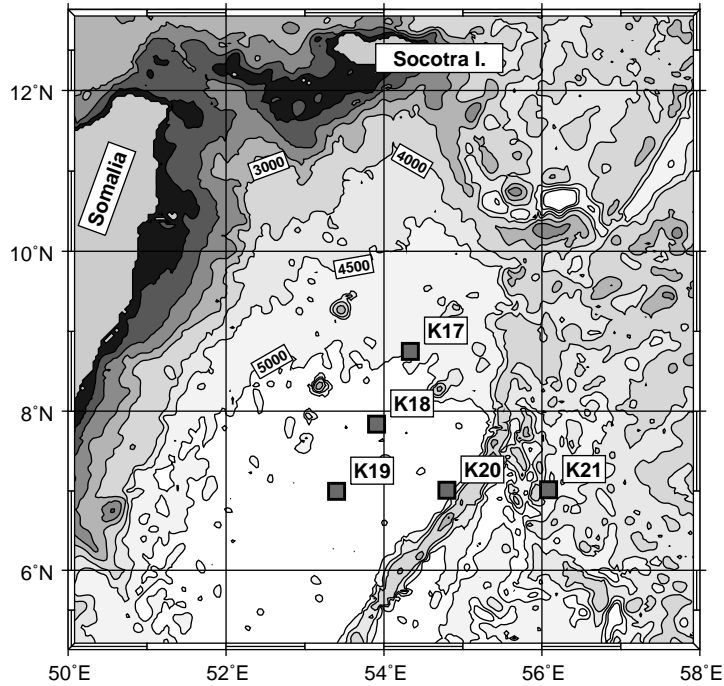


Fig. 1. Bathymetric map of the Somali Basin; depths in meters. Locations of moorings K17–K21 are shown by solid squares. The Chain Ridge is the bathymetric feature extending south from mooring K20.

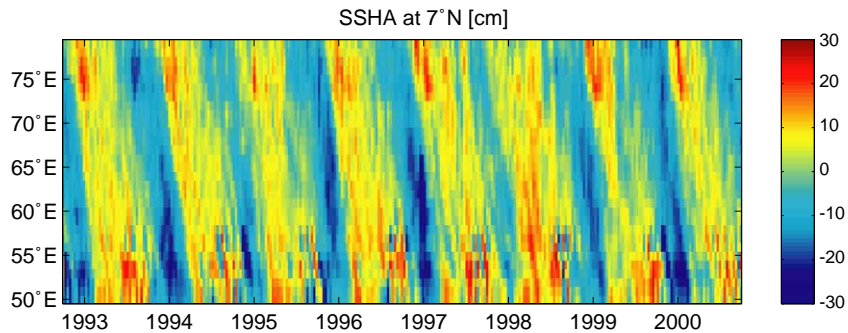


Fig. 2. Longitude–time plot of TOPEX/POSEIDON SSHA at 7°N.

became evident. Fig. 3 shows the high-pass filtered SSHA data, with a cut-off period (half-power point) of 115 days, for the year 1995. The monthly to 2-monthly signals were particularly evident during late summer and fall. The phase velocity was around 25 cm/s, slightly decreasing with time.

Fig. 4 shows the average SSHA wavelet energy spectrum in a region close to the coast of Somalia

between 52°E and 60°E and 5°N and 11°N. Overall, there was considerable year-to-year variability in the fluctuation strength of the wavelet energy as well as in its distribution among the different periods. In late summer and fall of each year, strong signals were found at periods between 30 and 50 days; significant signals at larger periods were only present during some years. The spatial

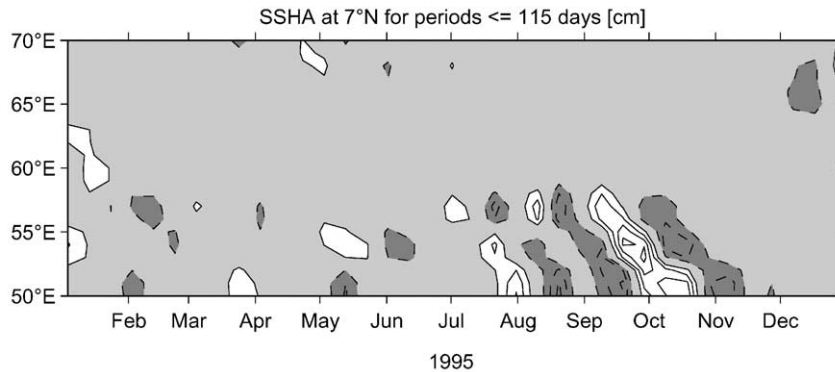


Fig. 3. Longitude–time plot of high-pass filtered SSHA data. SSHA smaller than -5 cm is dark gray shaded, SSHA larger than 5 cm is white. The contour levels are $\pm(5, 10, 15, 20)$ cm. Negative contour levels are drawn as dashed lines, positive contour levels as solid lines.

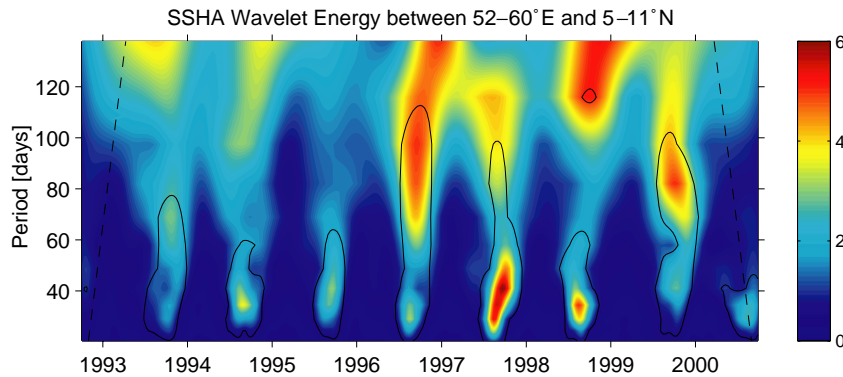


Fig. 4. Period–time plot of normalized SSHA wavelet energy averaged between $52\text{--}60^\circ\text{E}$ and $5\text{--}11^\circ\text{N}$. Solid lines mark the 95% significance level.

distribution of the SSHA wavelet energy at the period range between 38 and 45 days, corresponding to the central period range of the observed shorter-period fluctuations, is depicted in Fig. 5 for the different seasons of a mean annual cycle. High energy was found during summer and fall, while during winter and spring energy was relatively weak. Because significant SSHA wavelet energy signals at this period range are found only in the northern Somali basin, which holds for periods ranging from 30 to 120 days, we suggest a local generation mechanism for the observed waves.

This conclusion is in contrast with the interpretations of Anderson and Rowlands (1976) and Schott and Quadfasel (1982). These authors

suggested remote forcing of the Somali Current and GW by long planetary waves that reflected into short waves and led to an accumulation of energy near the boundary. However, such long waves, although associated with smaller velocities than the short waves, would still be associated with the same SSH variability and should thus be detected in our analysis. Since we do not see them in the interior of the Arabian Sea, the intraseasonal fluctuations must be generated locally in the Somali Current system.

The meridional dependence of the SSHA wavelet energy distribution is depicted in Fig. 6. The data were averaged between 52°E and 60°E for the period September–November. Also shown are the cut-off periods of freely propagating, first

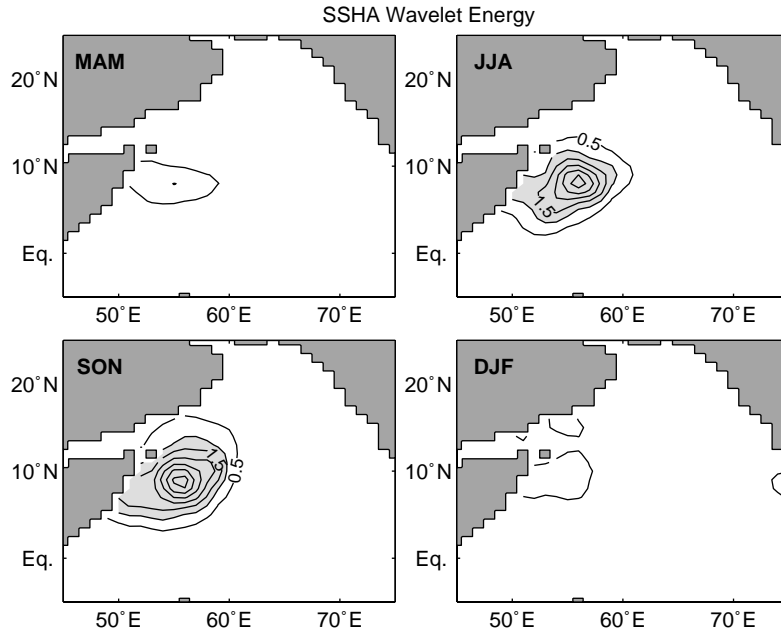


Fig. 5. Mean seasonal variation of the normalized SSHA wavelet energy at the period range 38–45 days. The light gray shaded areas mark the regions with a significance level higher than 95%.

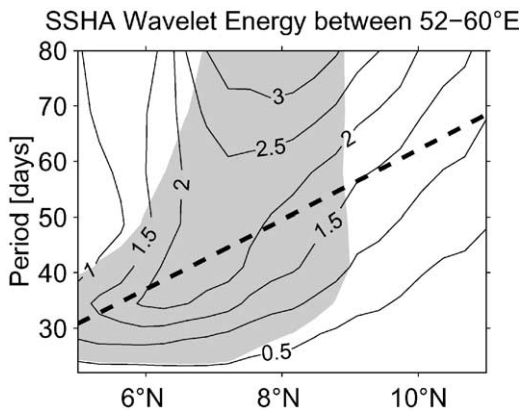


Fig. 6. Normalized SSHA wavelet energy as function of period and latitude averaged between 52°E and 60°E and for the 3-month period September–November. The gray shaded areas mark the regions with a significance level higher than 95%. The thick dashed line represents the cut-off period of freely propagating, first baroclinic mode, linear Rossby waves for a first mode internal gravity wave phase velocity of 2.64 m/s.

baroclinic mode, linear Rossby waves, which increase from about 30 days at 5°N to about 70 days at 11°N. They were computed for a density

structure typical of the area, taking a first mode, internal gravity wave phase velocity of $c_1 = 2.64$ m/s. In agreement with this theoretical trend, the observations show that the latitude where the energy reaches its maximum increased for increasing periods. South of 7°N, the energy maximum coincides with the Rossby wave cut-off period. However, significant fluctuation energy was also present in the lower range, where free baroclinic, linear Rossby waves cannot exist.

3. In situ observations

The in situ data were collected in the southwestern Arabian Sea from April 1995 to October 1996 by moorings carrying Aanderaa rotor current meters for measuring deep currents and temperatures. A detailed description of this observational program as well as of many aspects of the monsoon circulation in this part of the Indian Ocean has been given by Schott et al. (1997), Schott and Fischer (2000), and Dengler et al. (2002). Here, we use data obtained from the

moorings K17–K21 deployed in the central Somali Basin (see Fig. 1). They were part of a triangular setup specifically conceived to capture planetary waves propagating in this region.

A representation of the vertical structure of the measured horizontal velocity is given in Fig. 7 for depth levels 400, 2000, and 4000 m, showing that the current field was mainly composed of strong fluctuations (this is also characteristic for the records from the other four moorings). The fluctuations at the upper level were most pronounced during July–January, with a minimum in amplitude during the transition from the Northeast to the Southwest Monsoon. At 4000 m water depth, the currents were aligned in a northeast–southwest direction, which was due to the constricting bottom topography associated with the Chain Ridge (Fig. 1). Amplitudes of the deep velocity fluctuations above 5 cm/s were also found at the other moorings in the northern Somali basin (Dengler et al., 2002).

The results of a wavelet analysis carried out on the meridional velocity components measured at 400 m water depth at moorings K17–K19 are shown in Fig. 8. The normalized wavelet energy was calculated as function of period and time. The wavelet transform we used is similar to the one described above, but the normalization was performed by dividing each time-series by its own variance. At the southern mooring (K19), maximum oscillation amplitudes during October are found at periods of about 40 days. As time progressed, the periods became longer, reaching 55 days during the late Northeast Monsoon. At the two moorings further north, K17 and K18, the trend in time towards longer periods was even more pronounced and maximum oscillation amplitudes at periods of up to 90 days were seen (Fig. 8c). The onset of the strong fluctuations in the north occurred later in the Southwest Monsoon. A similar but noisier result was obtained when analyzing the zonal velocity components.

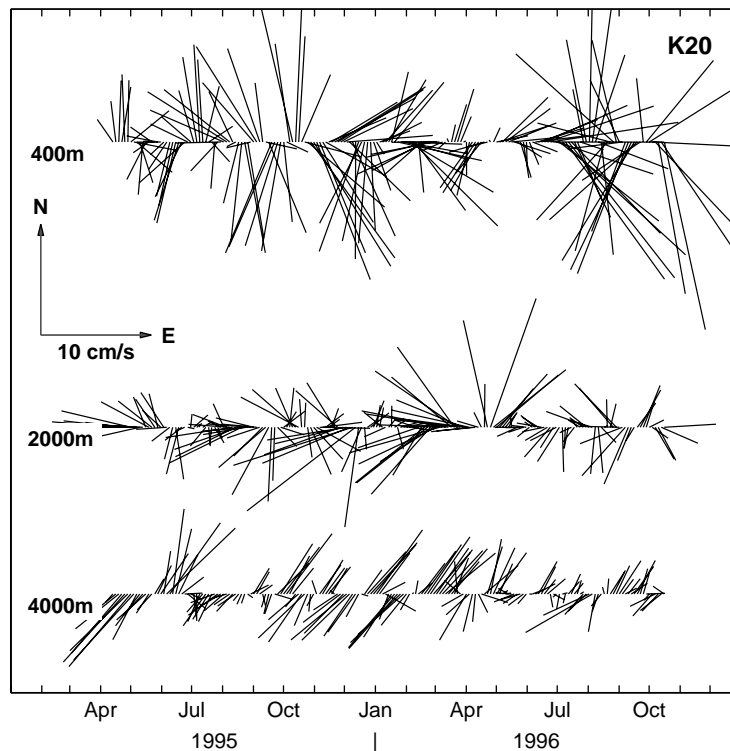


Fig. 7. Stick plots of 3-day averaged velocity data at the mooring K20 at 400, 2000, and 4000 m water depth. The location of the mooring is given in Fig. 1.

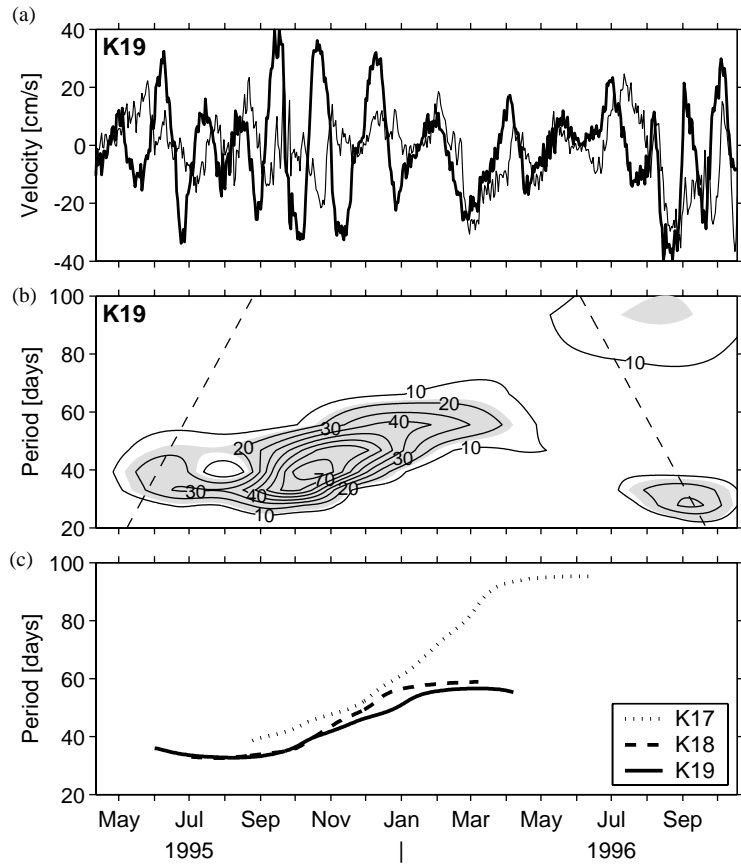


Fig. 8. (a) Time-series of zonal (thin solid line) and meridional (thick solid line) velocity at 400 m depth at mooring K19, (b) period–time plot of normalized meridional velocity wavelet energy at 400 m depth at mooring K19, and (c) periods of maximum oscillation amplitude at 400 m depth at the three moorings K17–K19. The light gray shaded areas in (b) mark the regions with a significance level higher than 95%. The curves shown in (c) are plotted only in these regions. The locations of the moorings are given in Fig. 1.

The temperature records measured at the five moorings at 2000 m water depth (Fig. 9) also showed large oscillations up to 0.4°C amplitude, with similar time-scales as the current fluctuations. Given the typical stratification in the area, such temperature variability corresponds to oscillation amplitudes of the isopycnals at this depth level of about 100 m. Instruments at levels higher up in the water column also showed these signals, albeit more obscured by noise. From July 1995 to February 1996 these temperature fluctuations were very similar over the mooring array, indicating the presence of large-scale baroclinic waves.

Characteristics of the observed waves can be quantified by calculating a local dispersion rela-

tion. This is ambiguous since the oscillation periods change both in time and in meridional space. For our estimate, we used the time-series of the meridional velocity at 400 and 700 m water depth, and the 2000 m temperature records. We selected these data sets because they were available for at least four of the five moorings. Periods were simply calculated as the temporal interval between two successive maxima or minima in the respective time-series. Phase differences and velocities were calculated by identifying corresponding extreme values in the different time-series. From our earlier analysis of the altimeter data, we know that the zonal phase speeds were of the order 20–30 cm/s, which narrows the range of possible solutions.

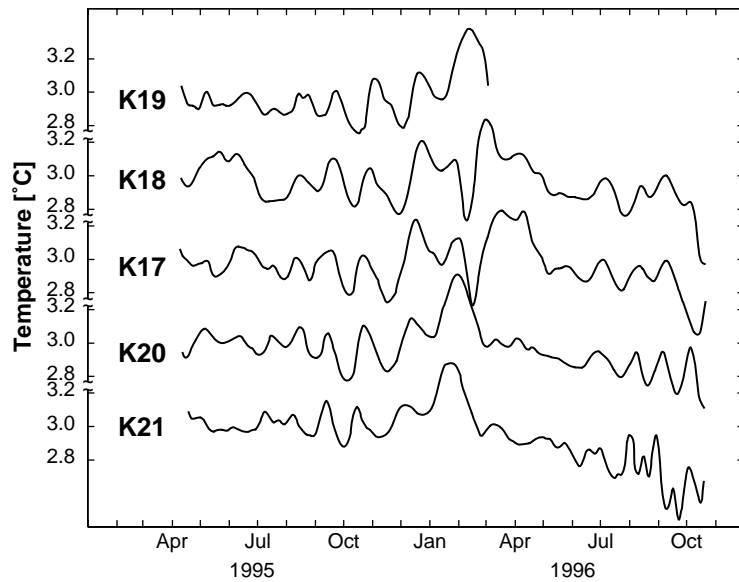


Fig. 9. Time-series of temperature at 2000 m water depth at the five moorings K17–K21. The locations of the moorings are given in Fig. 1.

Once periods and phase velocities were estimated, the corresponding wavelengths were calculated.

Fig. 10 summarizes these estimates. The fluctuation periods were smallest between July and August and increased steadily until January (Fig. 10a). Although the scatter in the data was quite large (the standard deviation varies between 3 and 10 days), the obtained trend corresponds well with trends obtained from the wavelet analysis presented in Fig. 8. The zonal phase velocity of the fluctuations, calculated from the K19–K21 records, was maximum in July (about 40 cm/s towards the west) and decreased strongly until October (about 15 cm/s; Fig. 10b). Such clear time-dependence cannot be identified in the evolution of the zonal wavelength, but there was also an indication of a decrease from 1000 to 500 km in the period from July to October (Fig. 10c). The meridional phase velocity of the fluctuations was calculated from the whole data set obtained from K17–K21. Since the main phase propagation was towards the west and the oscillation period changed with latitude, the errors associated with our visual estimates led to larger scatter in the resulting meridional phase velocity. Nevertheless, in general, the meridional phase

velocity was directed southward, its magnitude being about 20 cm/s (Fig. 10d). Similar to the zonal wavelengths, the calculated meridional wavelengths ranged between 500 and 1000 km (Fig. 10e).

A comparison between observed and theoretical dispersion relation is presented in Fig. 11. The theoretical dispersion relation we used refers to freely propagating, first baroclinic mode, linear Rossby waves. Their frequency is defined as

$$\omega = \frac{-\beta k_x}{k_x^2 + k_y^2 + f^2/c_1^2} \quad (1)$$

where β is the variation of the local Coriolis parameter f with latitude, k_x and k_y are the zonal and meridional wave numbers, respectively, and c_1 is the phase velocity of first mode internal gravity waves. This phase velocity was calculated from the local stratification measured in the area and resulted in $c_1 = 2.64$ m/s. For the meridional wave number we chose $k_y = 2\pi/800$ km. The resulting frequencies were not very sensitive to this latter choice.

Almost all frequencies calculated from the observations were above the corresponding theoretical ones (Fig. 11a). When plotting the

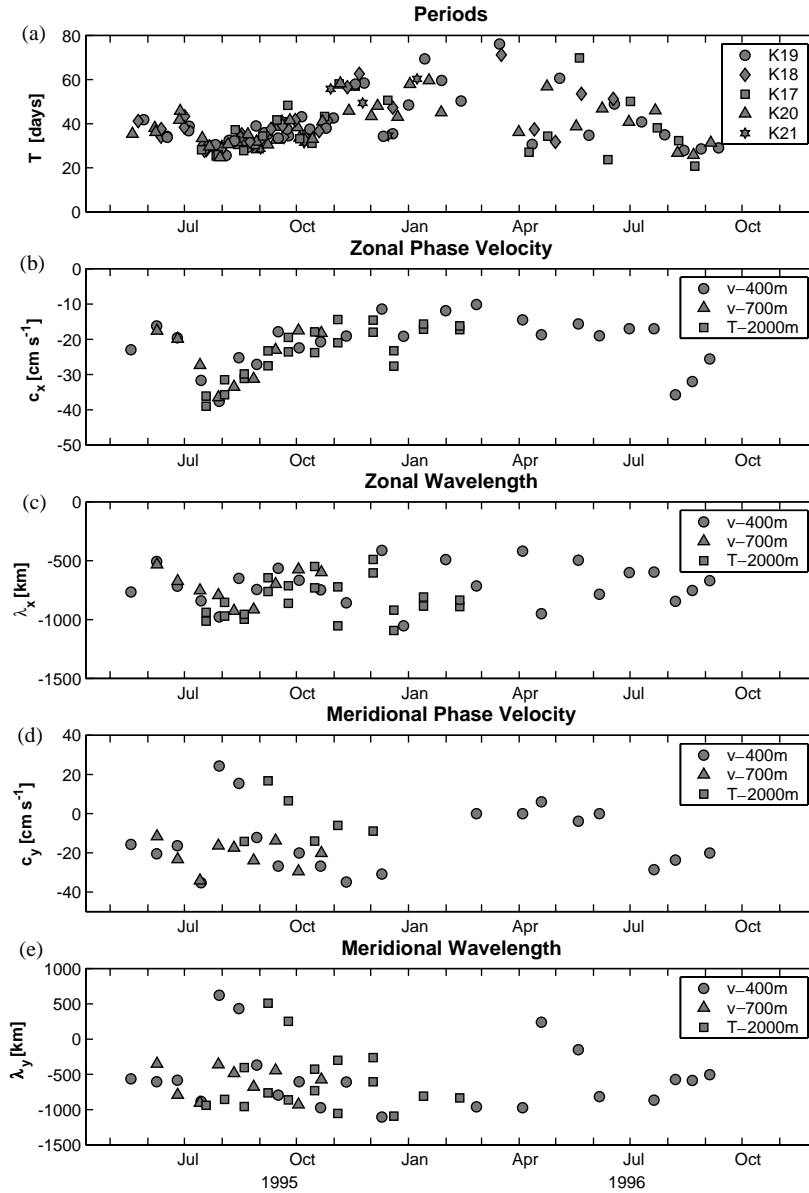


Fig. 10. Periods (a), zonal phase velocity (b), and zonal wavelength (c), meridional phase velocity (d), and meridional wavelength (e) as calculated from meridional velocity time-series at 400 and 700 m water depth as well as from temperature time-series at 2000 m water depth. Zonal phase velocity and zonal wavelength are calculated using data from the three moorings K19–K21. The other parameters are calculated using data from all moorings. The locations of the moorings are given in Fig. 1.

differences between observed and theoretical frequencies as function of time, it becomes evident that the largest deviations are found at the end of July, as also seen in the altimeter data, and that these steadily decreased until December. This

suggests that the observed fluctuations emerged during July and evolved toward freely propagating Rossby waves. The observed values were close to the wavelength where the maximum frequency in the theoretical dispersion relation (Fig. 11a)

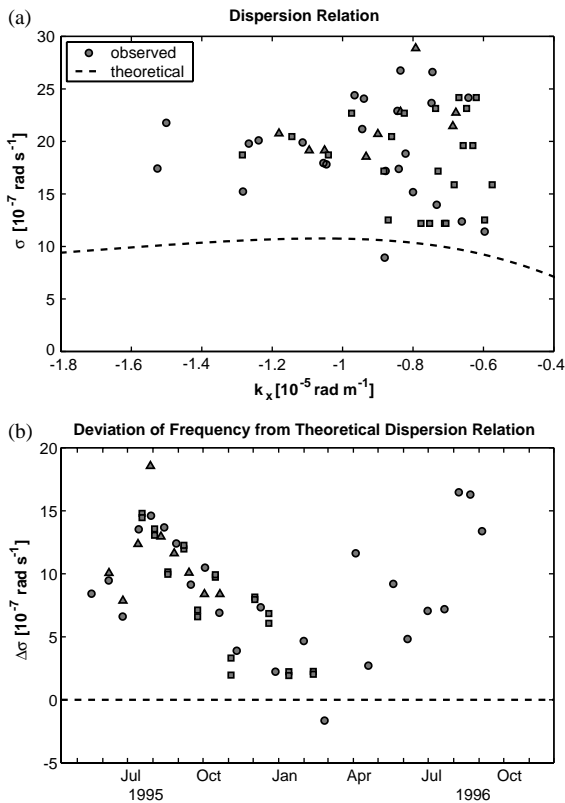


Fig. 11. Observed (symbols) and theoretical (dashed line) frequencies as function of zonal wave number (a) and deviation between observed and theoretical frequencies (b) as function of time. The theoretical dispersion relation corresponds to freely propagating, first baroclinic mode, linear Rossby waves assuming an observed first mode internal gravity wave phase velocity of $c_1 = 2.64 \text{ m/s}$ and a meridional wavenumber of $2\pi/800 \text{ km}$. The dots and triangles correspond to meridional velocity observations at 400 and 700 m, respectively, and the squares to temperature observations.

occurs. Here, Rossby waves are characterized by a minimum in their zonal group velocity. Since our data suggest a general southward phase velocity (Fig. 10d), this corresponds to northward energy propagation.

4. Summary and discussion

In this paper we presented an analysis of intraseasonal fluctuations in the southwestern Arabian Sea, based on altimetric SSHA data and

in situ current and temperature data from moored instrumentation. The region is very energetic and characterized by the GW during the Southwest Monsoon.

The analysis of the 8-year altimetric dataset shows

- that in late summer and fall of each year, strong propagating SSHAs exist with periods between 30 and 50 days, and during some years periods are up to 100 days,
- that the fluctuation energy is concentrated in the northern Somali basin, which suggests a local generation mechanism, and
- that a substantial part of this energy corresponds to wave periods well below the theoretical cut-off period of freely propagating, baroclinic Rossby waves.

The analysis of the in situ data from the triangular mooring array deployed from April 1995 to October 1996 in the southwestern Arabian Sea shows

- that strong current and temperature fluctuations are present throughout the water column, with current fluctuations as strong as 10 cm/s near the bottom,
- that the observed fluctuation periods are smallest at the end of July 1995 and increase steadily until January 1996,
- that the observed phase velocities have a westward component, strongly decreasing from the end of July until October 1995, as well as a southward component,
- that the energy of the observed waves propagates northward,
- that the observed wave periods are mostly well below the theoretical cut-off period of freely propagating, baroclinic Rossby waves, and
- that the deviation between observed and theoretical periods is largest at the end of July, during the first stage of the wave evolution, but decreases as time progresses.

The interesting question now, of course, concerns the generation of these waves and their possible interaction with the GW. The local

concentration of the energy in the northern Somali Basin rules out remote forcing effects through the wind, as explored in earlier studies (Anderson and Rowlands, 1976). Local wind fluctuations also could generate such fluctuations, but an analysis of the wind curl over the Arabian Sea failed to show such a concentration of fluctuation energy in the region (Fig. 12). Although the wind-curl wavelet energy in the period range between 38 and 45 days is relatively high during the Southwest Monsoon, it is mainly concentrated in the northern Arabian Sea. Slightly increased wavelet energy is also found at about 8°N and 60°E during June–August. However, the mismatch in the pattern of the SSHA and wind-curl wavelet energy (cf. Figs. 5 and 12) as well as the inferred northward energy propagation rules out the wind-curl fluctuations as a dominant source of energy in the intraseasonal oceanic variability of the southwestern Arabian Sea.

This conclusion is consistent with a study by Sengupta et al. (2001), who found similar oceanic fluctuations using a numerical model of the Indian

Ocean forced only with seasonal winds. They proposed hydrodynamical instabilities as the most likely generation mechanism. This seems reasonable, as the fluctuations develop with, but not before, the onset of the Southwest Monsoon, when the Southern Gyre and the GW are building up. A likely energy source for the fluctuations is the boundary between the Southern Gyre and the GW at around 4–5°N. Here, vertical shears of up to 3 m/s per 100 m have been observed already during relatively early stages of the monsoon (Leetmaa et al., 1982; Swallow et al., 1983). The lower boundary of this energetic layer rises from more than 100 m depth in the Southern Gyre to the surface in the transition zone to the GW and to more than 200 m in its center. The associated reversal of the meridional gradient of potential vorticity allows baroclinic instabilities to develop. Length scales of such baroclinic instabilities would then be 500 km or longer (Pedlosky, 1987; Cushman-Roisin, 1994). Likewise, the horizontal shear in this region is large, up to 4 m/s over less than 100 km, and the second meridional derivative of

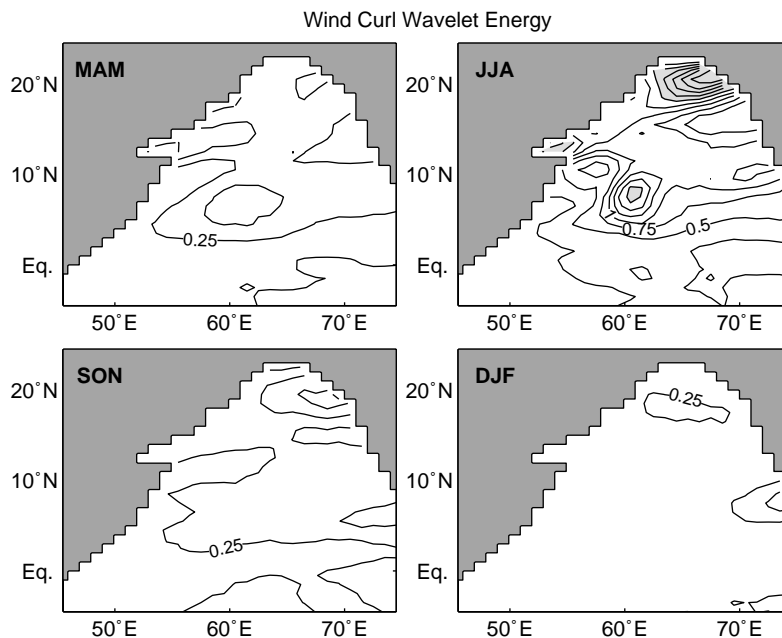


Fig. 12. Mean seasonal variation of the normalized wind-curl wavelet energy at the period range 38–45 days. The light gray shaded areas mark the regions with a significance level higher than 95%. Here, we used weekly wind data for the period October 1992–October 2000 that was acquired by the scatterometers aboard the European Remote Sensing Satellites (ERS-1 and ERS-2).

the zonal flow disappears in part of the domain, allowing barotropic instabilities to develop. Here, associated length scales would be an order of magnitude larger than the extent of the shear zone, i.e. 500–1000 km (Kundu, 1990; Cushman-Roisin, 1994). Both barotropic and baroclinic instabilities are thus capable of generating current fluctuations of the observed scales, but our data do not allow us to distinguish between them. The strong nonlinearities and the closeness of the region to the equator do not allow us to apply plain linear theory. The highly variable background stratification alters the potential vorticity gradient making it to deviate from the simple planetary beta. Doppler shifts due to the strong mean currents will alter the dispersion relation and it is therefore somewhat surprising how close the observed waves follow linear theory. The details of the dynamical interaction between mean and fluctuating flow cannot be resolved and quantified from the data set on hand, and an answer might only be found using high-resolution numerical modeling. However, the analysis of the 8-year altimetric dataset shows strong interannual variability of the intra-seasonal fluctuations, which are possibly related to the GW dynamics and in particular to its decay or collapse. A numerical study showed that besides the external forcing, the chaotic nature of the ocean dynamics contribute substantially to the interannual variability in the southwestern Arabian Sea (Wirth et al., 2002).

Acknowledgements

We express our gratitude to CNES/NASA and AVISO/Altimetry for provision of TOPEX/POSEIDON ‘SLA’ altimeter data and to Institut Français de Recherche pour l’Exploitation de la Mer (IFREMER) for provision of wind data. Critical comments of three anonymous reviewers helped with the revision of the manuscript. Financial support was obtained by the Bundesminister für Bildung und Forschung, Bonn, Germany under grant 03F0246A. The mooring work was carried out from R.V. *METEOR* under funding from Deutsche Forschungsgemeinschaft.

References

- Anderson, D.L.T., Rowlands, P.B., 1976. The Somali Current response to the Southwest Monsoon: the relative importance of local and remote forcing. *Journal of Marine Research* 34, 395–417.
- AVISO, 1998. AVISO User handbook for sea level anomalies (SLA’s), AVI-NT-011-312-CN, Edition 3.1. CLS Space Oceanography Division, Toulouse, France, p. 24.
- Brandt, P., Stramma, L., Schott, F., Fischer, J., Dengler, M., Quadfasel, D., 2002. Annual Rossby waves in the Arabian Sea from TOPEX/POSEIDON altimeter and in situ data. *Deep-Sea Research II* 49, 1197–1210.
- Cushman-Roisin, B., 1994. *Introduction to Geophysical Fluid Dynamics*. Prentice-Hall, Englewood Cliffs, NJ, 320 pp.
- Dengler, M., Quadfasel, D., Schott, F., Fischer, J., 2002. Abyssal circulation in the Somali Basin. *Deep-Sea Research II* 49, 1297–1322.
- Emery, W.J., Thomson, R.E., 2001. *Data Analysis Methods in Physical Oceanography*. Elsevier, Amsterdam, 638 pp.
- Evans, R.H., Brown, O.B., 1981. Propagation of thermal fronts in the Somali Current system. *Deep-Sea Research* 28A, 521–527.
- Fischer, J., Schott, F., Stramma, L., 1996. Currents and transport of the Great Whirl–Socotra Gyre system during the summer monsoon, August 1993. *Journal of Geophysical Research* 101, 3573–3587.
- Fu, L.-L., Christensen, E.J., Yamarone, C.A., Lefebvre, M., Menard, Y., Dorrer, M., Escudier, P., 1994. TOPEX/POSEIDON mission overview. *Journal of Geophysical Research* 99, 24369–24381.
- Kundu, P.K., 1990. *Fluid Mechanics*. Academic Press, Orlando, 638 pp.
- Leetmaa, A., Quadfasel, D.R., Wilson, D., 1982. Development of the flow field during the onset of the Somali Current, 1979. *Journal of Physical Oceanography* 12, 1325–1342.
- Lighthill, M.J., 1969. Dynamic response of the Indian Ocean to the onset of the Southwest Monsoon. *Philosophical Transactions of the Royal Meteorological Society A* 265, 45–92.
- Pedlosky, J., 1987. *Geophysical Fluid Dynamics*, 2nd Edition. Springer, New York, 710 pp.
- Schott, F., 1983. Monsoon response of the Somali Current and associated upwelling. *Progress in Oceanography* 12, 357–381.
- Schott, F., Fischer, J., 2000. Winter monsoon circulation of the northern Arabian Sea and Somali Current. *Journal of Geophysical Research* 105, 6359–6376.
- Schott, F., McCreary, J.P., 2001. The monsoon circulation of the Indian Ocean. *Progress in Oceanography* 51, 1–123.
- Schott, F., Quadfasel, D., 1982. Variability of the Somali Current system during the onset of the SW monsoon. *Journal of Physical Oceanography* 12, 133–141.
- Schott, F., Fischer, J., Garternicht, U., Quadfasel, D., 1997. Summer monsoon response of the northern Somali Current, 1995. *Geophysical Research Letters* 24, 2565–2568.

- Schott, F., Dengler, M., Schoenefeldt, R., 2002. The shallow overturning circulation of the Indian Ocean. *Progress in Oceanography* 53, 57–103.
- Sengupta, D., Senan, R., Goswami, B.N., 2001. Origin of intraseasonal variability of circulation in the tropical central Indian Ocean. *Geophysical Research Letters* 28, 1267–1270.
- Swallow, J.C., Bruce, J.G., 1966. Current measurements off the Somali coast during the southwest monsoon of 1964. *Deep-Sea Research* 13, 861–888.
- Swallow, J.C., Fieux, M., 1982. Historical evidence for two gyres in the Somali Current. *Journal of Marine Research* 40 (Suppl.), 747–755.
- Swallow, J.C., Molinari, R.L., Bruce, J.G., Brown, O.B., Evans, R.H., 1983. Development of near-surface flow pattern and water mass distribution in the Somali Basin in response to the Southwest Monsoon of 1979. *Journal of Physical Oceanography* 13, 1398–1415.
- Torrence, S., Compo, G.P., 1998. A practical guide to wavelet analysis. *Bulletin of the American Meteorological Society* 79, 61–78.
- Wirth, A., Willebrandt, J., Schott, F., 2002. Variability of the Great Whirl from observations and models. *Deep-Sea Research II* 49, 1279–1295.